INDIAN JOURNAL OF SCIENCE AND TECHNOLOGY

RESEARCH ARTICLE

Synthesis and Characterization of Bismuth Borate-Barium Titanate Glass Ceramics

T Sravan Rao[1], N V Prasad[1], Md Shareefuddin[1], G Prasad[1]*

1 Materials Research Laboratory, Department of Physics, Osmania University, 50007, Hyderabad, India

OPEN ACCESS

Received: 28.02.2022

Accepted: 15.03.2022

Published: 19.05.2022

Citation: Rao TS, Prasad NV, Shareefuddin M, Prasad G (2022) Synthesis and Characterization of Bismuth Borate-Barium Titanate Glass Ceramics . Indian Journal of Science and Technology 15(17): 839-849. https://doi.org/10.17485/IJST/v15i17.434

* **Corresponding author**.

gudurup@gmail.com

Funding: None

Competing Interests: None

Published By Indian Society for Education and Environment (iSee)

ISSN
Print: 0974-6846
Electronic: 0974-5645

Abstract

Objectives: In the present investigation, transparent novel glass embedded with ferroic matrix was prepared by melt-quenching method. Among all the glasses, selective glass ceramic is also prepared. Optical and electrical measurements were carried out on the samples. **Methods:** We have prepared the transparent glass composition of (100-x)[0.55Bi_2O_3-0.30B_2O_3-0.15TiO_2] +x$BaTiO_3$, with x=0, 10, 20, 30, 40, 50 wt.%. Appropriate amounts of reactant mixture were well mixed in agate mortar and melted in a porcelain crucible. The composition is quickly quenched by pouring on pre-heated stainless-steel plate and pressed with another plate. Differential Thermal Analysis was made on the glasses. Detailed optical absorption and impedance measurements were made on the said above glass matrix. **Findings:** From the XRD spectra, amorphous and crystalline nature was established on the glass and glass ceramic sample. Optical absorption spectra show that with increasing the $BaTiO_3$ in the glass matrix, it results into structural compactness by means of non-bridging oxygen. The results are consistent with the oxygen packing density values. Impedance spectroscopic plots have shown broad peaks and therefore these materials are being considered as special type multicomponent glass ceramics. Disorder nature of the samples was also discussed with the help of dc-conductivity plots. Among all the samples, 60-BBT-40BT has shown broad spectroscopic peak. Therefore, this sample was annealed at 700^oC, and the XRD pattern resembles with $Bi_4Ti_3O_{12}$ Aurivillius phase, instead of $BaTiO_3$ phase. Detailed impedance measurements were also made on the glass ceramic. **Novelty:** Dielectric ceramic-glass are being used to fabricate energy storage capacitors; however, further studies are needed in order to improve pore-free microstructures. In view of this, transparent glass matrices are embedded with ferroic materials namely $BaTiO_3$ and the combined optical and electrical results would be useful for future promising optoelectronic materials by means of one-to-many applications.

Keywords: Ferroelectric; glassceramics; optical absorption; impedance; dielectric; FTIR

1 Introduction

Ferroic materials have attracted much attention due to its domain characteristic feature and temperature dependent macroscopic properties such as phase transition, coupling properties etc. In addition, ferroic materials form an essential subgroup of functional or smart materials whose physical properties are sensitive and changes with the external conditions such as temperature, pressure, electric, and magnetic fields. The most important and striking feature of ferroic material is its spontaneous polarization (the material posses' polarization without any applied electric field). Due to the fact of this, these substances are considered to be high-energy–density materials (to store and release energy). Finally, in a well-regulated manner, one can make these materials as highly useful sensors and actuators [1,2]. Recent reports on phosphate-lithium, sodium borate silicate embedded with chromium oxide glasses and cadmium lead phosphate glasses have shown interesting radiation/ neutron shielding applications [3–6]. Among all the ferroelectric perovskite oxides, $BaTiO_3$ is the most investigated material in the last few decades because of its intrinsic ferroelectric properties, they have shown promising applications in the fields of electroceramics, especially in microelectronic, dielectric and multilayer capacitors, ultrasonic transducers, positive temperature coefficient (PTC) resistors, pyroelectric infrared sensors etc. It is a known a fact that the borosilicate glasses have strong network and easily can be doped with any oxide materials [7,8]. In addition, multiferroic materials belonging to the Aurivillius family have shown high coupling (magnetoelectric) coefficient [9]. Another important material of Aurivillius family is Bi_4Ti3O_{12}. It is a well-known Ferroelectric Random-Access Material (FRAM). In addition, $Bi_4Ti_3O_{12}$ has higher transition temperature and above the phase transition temperature (T_c~675^0C) it turns from orthorhombic to tetragonal [10].

Ferroelectric glass ceramics exhibit unusual ferroelectric properties owing to the fact of its ceramic-glassy nature. Due to its characteristic nature of energy-storage applications, many Indian researchers have been concentrating in this direction [11,12].

Glass matrices are being prepared by means of solid-state route, sol-gel, hydrothermal route etc. However, it is difficult to choose the above-mentioned process due to many constraints involved in the reaction process. Recently many researchers have concentrated on $BiFeO_3$, Pb-based, Bi_2O_3 and Fe_2O_4 glasses [13–17]. Bismuth based glass ceramics are used in the fabrication of electronic and semiconducting devices. However, further improvements are needed to prepare pore free micro structures. In addition, very few reports are available on electrical studies on glass ceramics. Keeping in view of importance of ferroelectric glass ceramics and to improve pore free microstructure, a systemic study on combined optical and electrical is needed in this direction.

In the present investigation, we are focusing on the $BaTiO_3$ based glass-samples. Prior to the BT preparation, we have fabricated Bi_2O_3-B_2O_3-TiO_2 (BBT) glass matrix, and embedded with $BaTiO_3$ (BT) by using the following composition (100-x) BBT-x BT (with x=0, 10, 20, 30, 40, 50 wt. %). It should be noted that Bi_2O_3 is very suitable for both network modifiers as well as network former. Therefore, high concentration of Bi_2O_3 is chosen in the present glass matrix composition. Moreover, recent reports revealed that the glass-ceramics have lower sintering temperature, compared to ceramics [11]. Among the entire glass samples, selective glass sample was crushed into powder and pressed into a pellet. The pellet glass ceramic sample was annealed at 700°C for 2 hours. Impedance measurements were made on all the samples and the results were discussed.

2 Methodology

Keeping in view of aforementioned importance, in the present study we have prepared transparent glass-materials. The ferroic-glass materials were prepared by melt-quenching method and the chosen composition is: (100-x)[0.55Bi_2O_3-0.30 B_2O_3-0.15TiO_2] +x$BaTiO_3$ (with x= 0,10,20,30,40,50 wt %). Appropriate amounts of Bi_2O_3, B_2O_3, TiO_2 and $BaTiO_3$ are well mixed in agate mortar and melted in a porcelain crucible for half-an-hour at 1100-1200°C depending on the $BaTiO_3$ concentration and then quickly quenched by pouring onto pre-heated stainless-steel plate and pressed with another plate (both maintained at 100^0C). The glass transition temperature is obtained from TGA analysis. The glass transition (T_g) and crystallization temperature (T_c) were found to be 450^0C and 525^0C respectively.

X-ray diffraction (XRD) peaks are recorded on the glass ceramics samples, using Pan Analytic X'pert plus diffractometer. The Cu-Kα(1.54 A) radiation is used and scanned in the range $10^0 \leq 2\theta \leq 80^0$ with a speed of 2^0/min. Densities of the glass ceramics are measured using Archimedes principle using xylene (density 0.87 gm/cm^3) as liquid media. Scanning electron micrographs of these samples are obtained with ZEISS EVO18 (special edition). Oxford system Energy Dispersive Spectroscopy (EDS) attached to the electron microscope is used for obtaining the EDS spectra. Fourier transform infrared (FTIR) spectra were recorded using FTIR-8400S Shimadzu. FTIR Spectra were obtained in the range of 400-2000 cm^{-1}. Optical absorption spectra were recorded using UV 3092 UV-VIS spectrometer. Differential Thermal Analysis (DTA) was carried out from room temperature to1000 ^{0}C at a rate of 10^0C/min, using DTG-60 Shimadzu. Among all the glass samples, 60BBT-40 BT glass was crushed into powder and pressed into a cylindrical pellet. Detailed impedance spectroscopic studies were also made on the glasses as well as glass ceramic sample, using Autolab (PGSTAT-30) Impedance analyzer. Prior to the electrical measurements,

silver paste was coated on both sides of the glass/ceramic pellets (or disks) for good electrical contact.

3 Results and Discussion

The XRD patterns shown in Figure 1, exemplifies the amorphous nature of the sample. The data presented in the Figure 1, reveal that the prepared glass samples have amorphous nature. Scattering observed at low Bragg angles, indicates disorder-lattice and this is being attributed to the amorphous characteristic nature of the glass. The crystalline nature of BT is not appeared in these samples. In the present study, the quenched samples have shown the amorphous nature, in spite of adding ferroelectric phase. However, the glass composition 60-BBT-40BT, annealed at 700^0C for 2 hours, has shown crystalline phase (Figure 1 g). The crystalline Bragg peaks were well-matched with the $Bi_4Ti_3O_{12}$ Aurivillius (layered perovskite) phase. The matched (h k l) values were mentioned in the Figure 1g. All glass samples were found to be transparent. The pure BBT transparent glass sample is shown in the Inset Figure 1 a. The ceramic pellet, made by the glass composition 60 BBT-40 BT, photograph is also shown as the inset Figure 1 g.

Figure 1 g shows the crystalline phase and this nature is attributed to the ionic conductivity of glass-ceramic matrix. It is a known fact that Aurivillius layer compounds, ($Bi_4Ti_3O_{12}$) have high ionic conductivity nature, due to the presence of oxygen vacancies. It should remember here that Bi^{+3} alone may not contribute high ionic conductivity in bismuth-based glasses and Bi-based glasses should not be compared with other Pb-based glasses [13,16]. Moreover, Bi^{+3} groups of ions have lone-pair electronic configuration, and they have two outer most orbits with a closed shell of Pyramidal bonding [18]. The pyramid posses a dipole moment and finally might lead to spontaneous polarization in these materials.

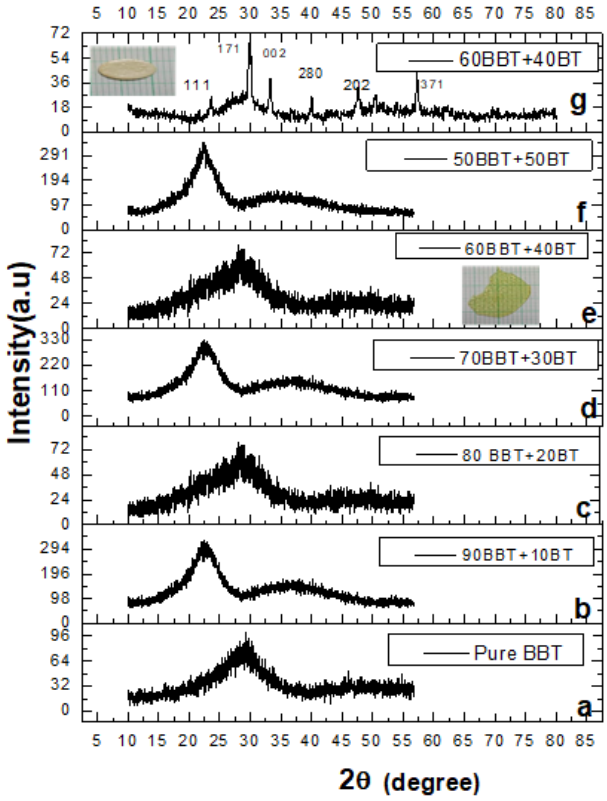

Fig 1. (a-f)XRD patterns of the Glass Composition of 100-xBBT- X BT (x=0,10,20,30,40,50) (g)XRD pattern of the glass composition 50BBT+50BT showing crystalline nature

The general formula of BLSF is described as $(A_{n-1}B_nO_{3n+1})^{2-}(Bi_2O_2)^{2+}$. The perovskite blocks are interleaved with $(Bi_2O_2)^{2+}$ layers. The bismuth ion situated at A-site in the perovskite structure and the ferroelectric properties are mainly attributed to strong covalent bonds of Bi-O [19]. The density and molar volume of transition metal ion concentration (N_i), Polaron radius

(r_0), interionic distance (R) and oxygen packing density (OD) values were calculated by using the following relations:

Density of the samples were calculated from the Archimedes Principle using the relation

$$\rho = \frac{w_a}{w_a - w_b} * \rho_b \tag{1}$$

Where ρ_b - is the density of the reference liquid (xylene=0.865 g/cc) and w_a & w_b represent the weight of the glass-ceramic samples measured in air and xylene respectively.

Molar Volume can be calculated by using the formula:

$$V_m = \frac{M_c}{\rho} \tag{2}$$

Is the molecular weight of the glass-ceramic

Transition metal ion concentration (N) can be calculated by using the relation

$$N = \frac{0.01\ X\ NA\ X\ \rho}{Vm} \tag{3}$$

Where N_A is Avogadro number and ρ is density and V_m are molar volume of the samples respectively. Polaron radius of the glass matrix is calculated by using the following formula

$$r_p = (\frac{1}{N})^{\frac{1}{3}} \tag{4}$$

The interionic distance of the constituent atoms is calculated by using the formula

$$r_i = \frac{1}{2}(\frac{\pi}{6N})^{\frac{1}{3}} \tag{5}$$

Here, N represents the transition metal ion concentration.

The above said calculation were made and summarized in the Table 1. From the Table 1, the molar volume of the glass materials was found to decrease with increasing the BT concentration in the glass-matrix. The decreasing nature of the molar volume is attributed to conversion from non-bridging oxygen atoms (NBO) to bridging oxygen atoms (BO) in the glass matrix. In TiO_6 octahedral structure, this kind of conversion is predominant in glass materials. The result is consistent with the optical studies of Ni-doped bismuth borate glasses[19] and lithium phosphate glasses[20]. The interionic distance between titanium is mainly dependent on the concentration of Ti ion. The interionic distance decreases with the increase of Ti concentration[20]. To extract more information on this, optical measurements were performed on these samples.

The Differential Thermal Analysis (DTA) is shown in Figure 2. The glass transition (T_g) and crystalline temperature (T_c) were obtained within the experimental errors. The endothermic and exothermic dips were found at 450^0C and 650^0C respectively. It is also noticed from the plot that Tg increases with the BT concentration. The increase of T_c indicates that the coordination nature of glass network former. An increase in T_g, with BT concentration, indicates the bond strength of network former. The difference between T_g and T_c is also found to be nearly 200^0C. The large difference between T_g and T_c shows that these glass materials are thermally very stable. The thermal stability of these compounds is attributed to the complex structure of the present ferroelectric glasses. In addition, the average interionic separation (r_i) and polaron radius (r_p) were calculated and given in the Table 1. From the values it is concluded that strong localized carriers predominate in the conduction process, as $r_p < r_i$.

Table 1. Depicting the Various Physical parameters- Density, Molar volume,Transition Metal Ion concentration, Polaron Radius, Inter Ionic Distance,Oxygen Packing Density, Optical Band Gap and Urbach Energy of different GlassCompositions

SL NO	Sample	Density (ρ) gm/cc	Molar Volume (VM) cc/mole	Transition Metal Ion Concentration (Ni) 1020/cc	Polaron Radius (rp) A^0	Inter Ionic Distance (ri) A^0	Oxygen Packing Density (OPD) g.atm/I	Eopt eV	Urbach Energy (ΔE) eV
1	Pure BBT	7.5209	40.6014	11.1568 X 1020	9.6416 X 10-16	3.8849 X 10 -16	197.0375	2.97	0.58

Continued on next page

Table 1 continued

2	90 BBT + 10 BT	7.0921	42.0382	10.1611 X 1020	9.9468 10-16	X	4.0078 10-16	X	261.6667	2.93	0.60
3	80 BBT + 20 BT	7.5726	38.4178	11.872 X 1020	9.444 10-16	X	3.8052 10-16	X	286.3251	2.98	0.52
4	70 BBT + 30 BT	7.4084	38.2952	11.6517 X 1020	9.5032 10-16	X	3.8291 10-16	X	287.2422	2.96	0.44
5	60 BBT + 40 BT	7.0631	39.1457	10.8673 X 1020	9.7265 10-16	X	3.9191 10-16	X	281.0041	2.98	0.58
6	50 BBT + 50 BT	6.873	39.1785	10.566 X 1020	9.8181 10-16	X	3.956 X 10-16		280.7662	3.01	0.75

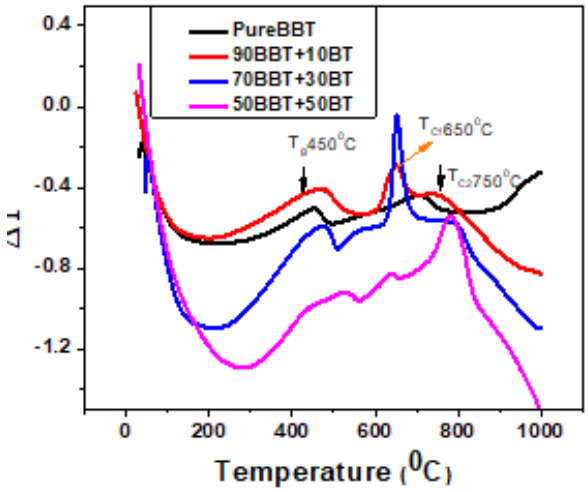

Fig 2. DT vs. temperature (°C) for all the glass compositions

The FTIR spectra of the present glass materials (100-x) BBT-x BT, obtained at room temperature in the spectral range of 400-2000 cm^{-1}, is shown in theFigure 3. Peaks observed at 860-869 cm^{-1} indicates the asymmetric stretching vibrations of Bi-O bonds of $[BiO_3]$Units[21,22]. The peaks associated 500-530 cm^{-1}, shown as inset Figure 3, is assigned to Bi-O bonding of BiO_6octahedral[23]. A shift in the peak maxima, observed with increasing the BT-composition, confirm the asymmetric stretching. Peaks appearing near 600 cm^{-1} clearly indicates Bi-O stretching vibration mode. The peaks at 750 cm^{-1} are ascribed to the B-O-B linkage network. Peaks appearing near 750 cm^{-1} are mainly due to the Ti-O-Ti symmetric stretching of TiO_4 units. Band appearing near 1100 cm^{-1} (IR region) is being attributed to B-O stretching vibrations of BO_4 tetrahedral network[24]. From the spectra, the peak at 1250 cm^{-1} is found to increase that with BT content in the glass composition. Peaks observed near 1450 cm^{-1} is attributed to asymmetric vibrations modes of non-bridging oxygen of B-O-B matrix. Bands assigned ~1549 cm^{-1} is attributed toB-O asymmetric stretching vibration of BO_3 units in meta-borate, pyro-borate and ortho-borate groups[24]. Band at 1632 cm^{-1} is due to metal-hydroxyl ion bonding[11]. From the overall spectra it is concluded that the presence of BT composition in the glass matrix certainly influencing the glass structure and acts as a network modifier.

Figure 4 shows the optical absorption spectra and Tauc plot. Figure 4 c shows Urbach Energy of the BBT-BT glass samples. From the UV-visible optical spectra, shown in Fig 4(a), the absorption coefficient is calculated by using the following formula:

$$\alpha = \frac{1}{d}\log\left(\frac{Io}{I}\right) \tag{6}$$

The term d represents thickness of the sample, Io and I represent the intensity of incident and transmitted light beam respectively.

The absorption coefficient is calculated by the following formula:

$$\alpha h\nu = [B(h\nu - E_g)]^2 \tag{7}$$

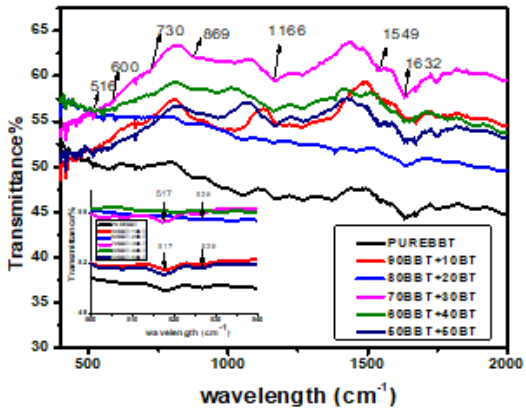

Fig 3. FTIR spectra of (100-x)BBT- (x)BT (x=0,10,20,30,40,50) (The peaks associated 500-530 cm^{-1} shown in inset)

The constant B is independent of energy (E), also known as tilting parameter.

The term hν represent the photon energy and υ index constant. The index constant can be 1/3, 1/2, 2, 3 and these values correspond to forbidden, direct allowed, indirect allowed, indirect forbidden respectively. However, in the present case, the index constant f_o fitted by1/2, therefore it is concluded that the bands are belong to direct band gap. The variation of $(\alpha h\nu)^{\upsilon}$ with hν, known as Tauc Plot, is shown in Figure 4 b. The values of E_g were estimated with help of the tau plots (Table 1). The values of E_g were calculated by extrapolating the linear region of the plot, which touches the X-axis. The optical band energies (E_g) were found to increase with increasing the BT composition. An increase in optical band gap energy is attributing to the conversion of Non-bridging oxygen's to bridging oxygen atoms. The variation of lnα with $\alpha h\upsilon$ is shown in Figure 4 c. The Urbach energy was evaluated from the plot and the values are summarized in Table 1.

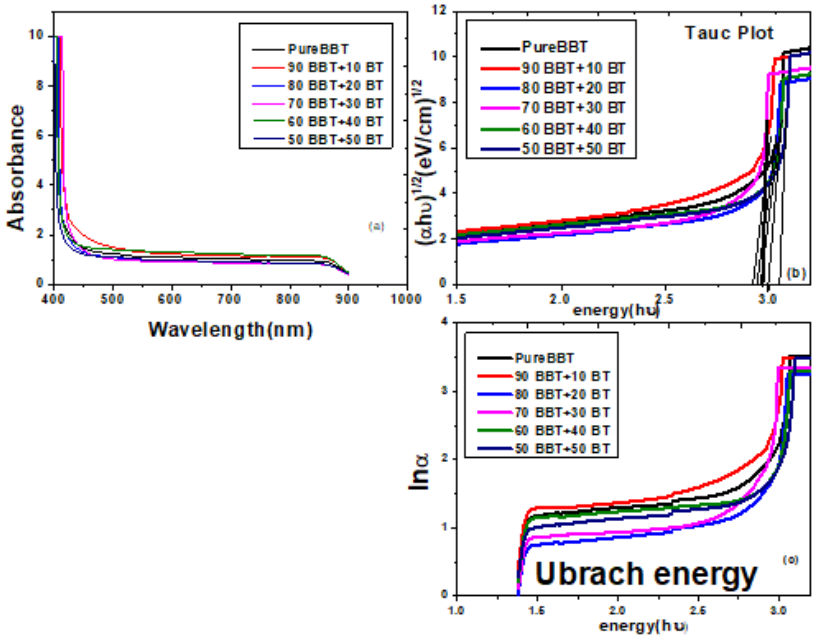

Fig 4. (a)Optical Absorption Spectra of all (100-x)BBT-(x)BT (x=0,10,20,30,40,50) (b)Tauc plots of the corresponding Glass Samples (c) Ina Vs energy (eV) or Urbach Energy (eV) of allGlass Compositions

The dielectric properties of the glass ceramics can be understood by means of combined impedance and modulus spectroscopic plots. Figure 5 shows the variation of Z" and M" with frequency for all the glass compositions, obtained at 125°C and 200°C respectively. From this plot, it is evident that the broad peaks found to increase with increasing the BT content. In addition, the maximum peak position is also found to shift towards right with increasing the BT-composition. The broad Z" peak also indicates the presence of multiple ions namely Bi, Ti and Ba in the glass matrix. All Z" values were found to merge into single value at higher frequency region. Observing higher Z" values at lower frequencies are being attributed to accumulation of space charges at grain boundary interfaces. Similar results were seen in lead calcium titanate borosilicate glasses [14]. Modulus also known as dielectric modulus which is inversely related to the permittivity (M"=1/€"; M*=M'- j M" here M' and M" represents real and imaginary part of modulus). Broad spectroscopic peaks observed in the intermediate frequency range clearly confirm the disorder nature of glass-materials. An interesting aspect in the modulus plot is that the M" increases suddenly at higher frequency region and this kind of behavior is mainly due to the increasing the ionic conductivity of the glass samples.

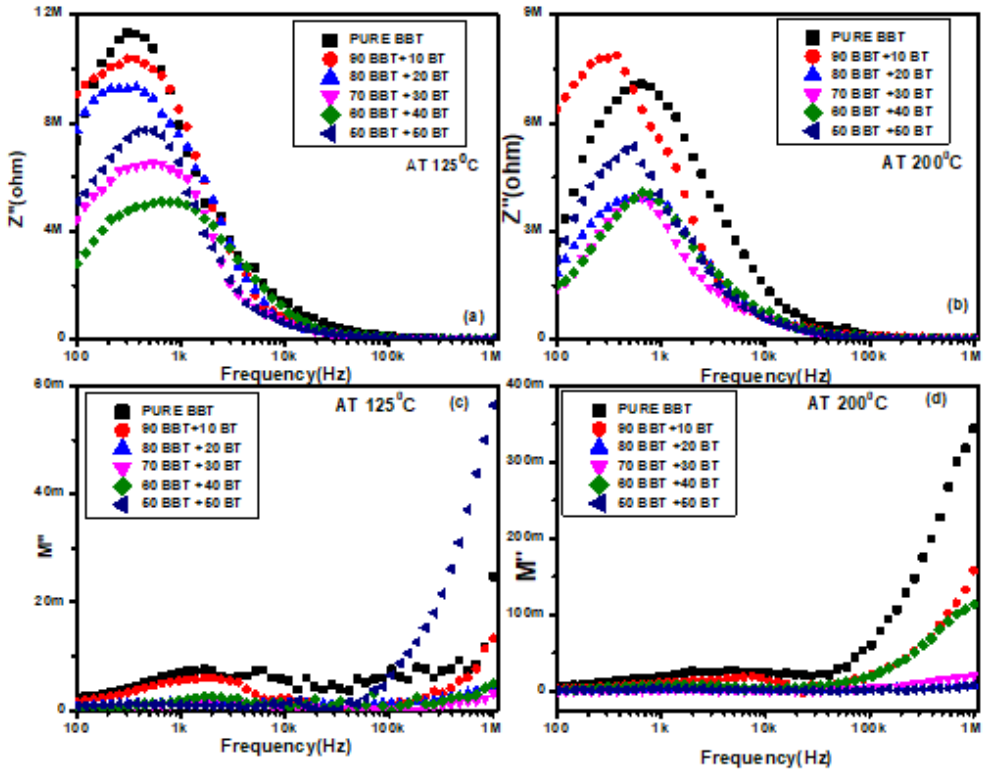

Fig 5. Variation of Z"(a&b) and M"(c&d) with frequency for all glass compositions at 125^{0}C and 200^0 C

Figure 6 shows the variation of ac-conductivity with frequency for all glass materials. The data was obtained at different temperatures, mentioned in the plot. From the plot it is clearly seen that the dispersion observed at low frequency region is found to increase with increasing the BT-composition in the BBT-BT glass matrix. From the plot, a sudden change in the conductivity near 125^{0}C is ascribed to the presence of oxygen vacancies [25]. For all compositions, M" approaches to zero at lower frequencies. Dispersion observed at liger frequency region and merging of ac-conductivity into single value at higher frequency is generally attributed to conduction mechanism assisted by short rage mobility of charge carriers [26].

Figure 7 shows the variation of dc-conductivity, obtained from the ac- conductivity data by extrapolating to 1 Hz frequency with inverse of temperature. From the dc-conductivity plot it is evident that the activation energy increases with the BT-composition. Moreover, the ac-conductivity is found to merge into single value at higher frequency domain. This nature clearly confirms the following hoping mechanism:

$$Ti^{+3} + e^{-} \rightarrow Ti^{4} \tag{8}$$

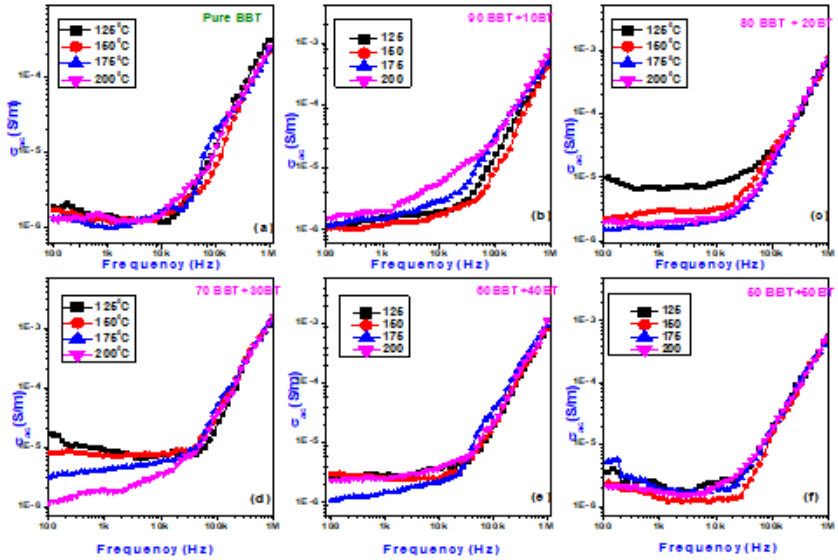

Fig 6. Variation of ac-conductivity with frequency for all glass compositions

The conductivity data is well fitted into Arrhenius Law and one can obtain activation energy from the slopes of the plots. The activation energy values, calculated from the slope of the dc-conductivity, were mentioned in the Figure 7. It is also evident that the activation energy values were found to be around 1 eV. From this one can speculate that Pure BBT sample has more oxygen vacancies and these vacancies participate in the role of conduction process. Figure 8 shows SEM photographs all the glass samples. From the plot it is evident that the grain size increases with BT-composition in the matrix. From this, one can speculate that BT composition has shown influence on the microstructure. Changes observed in the size, shape and mean crystalline size can also corroborated to the conduction phenomenon, where activation energy is found to increase with the BT composition. Similar results were seen in BT-based cadmium alkali borate glasses, where the glass density was found to increase with the BT composition. From this it is evident that TiO_2 plays glass former [23].

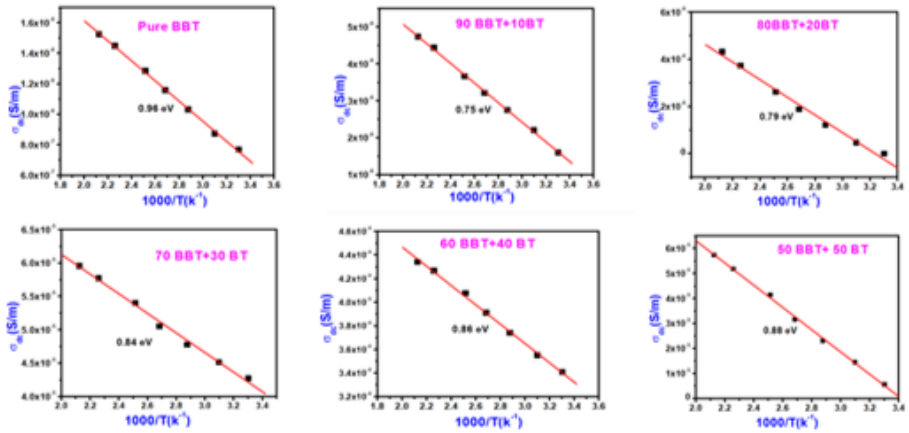

Fig 7. The activation energy values from the slope of thedc-conductivity for (100-x)BBT- (x)BT (x=0,10,20,30,40,50)

The variation of log Z" with frequency is shown in the Figure 9a. Two distinct slopes observed in Figure 9 b explains about grain and grain boundary contribution of the samples. Figure 9c demonstrates the variation of imaginary part of impedance (Z")

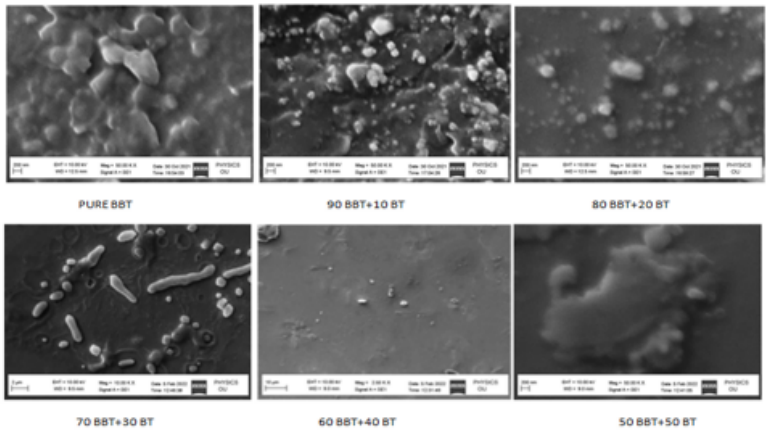

Fig 8. SEM images of all glass samples

with real part of impedance (Z') (Cole-Cole Plot) at 125° C. Observing an incomplete semicircle, and a spike like behavior at 125°C in the intermediate region is attributed to limited ionic conduction and the blocking capacitance of the sample. The ionic conduction is mainly due to the doubly ionized vacancies. This type of conduction process can be explained by the following Korger-Vink notation.

$$O_O x \rightarrow V'' - + 2e' + 1/2O_2 \tag{9}$$

Recent report of Zhao et al[26] on $BaCO_3$-TiO_2-Al_2O_3-SiO_2-CeO_2 revealed that the molten solution has shown BaTiO3 (BT) phase at higher temperature (>1200^{0}C). However, on the contrary, in the present investigation, BBT-glass matrix embedded with BT has shown $Bi_4Ti_3O_{12}$ (an alternative compound of BT). Based on the above reaction (equation 9), the source of conduction is through Ti^{4+} to Ti^{3+}. The released electrons get trapped at the defects such as V_o". It is also presumed that the conduction in glass ceramic is due to low doubly ionized vacancies (V_o") and stable oxygen vacancies. The results are consistent with increasing dc-activation energy values of all glasses. A sudden decrease in dc-activation energy of ceramic-glass sample clearly confirms the hopping of electron between the titanium ionic sites.

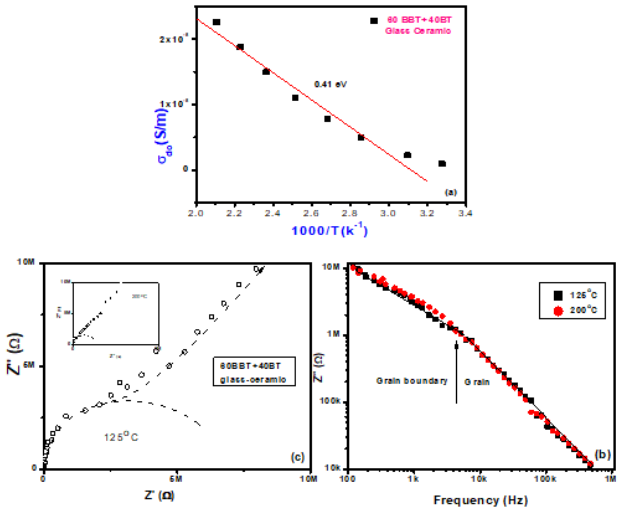

Fig 9. (a) The variation ofdc-conductivity for 60BBT+40 BT Glass Ceramic (b) Variation of Z"with frequency of the 60BBT+40 BT Glass Ceramic Sample (c) Cole-Cole plot of60BBT+40 BT Glass Ceramic Sample

4 Conclusions

The glasses with the composition (100-x) BBT-xBT, (where x=0, 10, 20, 30, 40, 50 wt. %) were prepared under controlled heat treatment process. Among all the composition, 60BBT-40BT has shown broad spectroscopic peak with lesser relaxation time. It is concluded that there is a decrease in the dipole concentration and moreover the sample has shown crystalline nature of $Bi_4Ti_3O_{12}$ phase instead of BT-phase. From the detailed ac-conductivity data and impedance, it can be concluded that excited Ti^{4+} ion reduces to Ti^{+3} ions by means of electron hopping mechanism. In addition, oxygen vacancies play role in the conduction process. Ac conductivity data follows Jonscher's power law. Broad asymmetric Z" peaks indicate different relaxation times. Decrease of Z" peak with the composition clearly indicate increase of dipole concentration. The trend of Dc conductivity confirms the mixed transition conductivity of hopping of electron and migration of oxygen vacancies. Thermal analysis also reveals that the stability of the glass compounds is due to bridging of oxygen network. The increasing order nature with BT clearly indicates that the chosen composition makes it a suitable candidate for ferroelectric applications.

References

1) Yadav AK, Gautam CR. A review on crystallization behavior of perovskite glass ceramics. *Advances in Applied ceramics*. 2014;p. 193–205. doi:10.1179/1743676113Y.0000000134.
2) Du X, Pu Y, Peng X, Zhang J, Ji J, Li R, et al. Optimizing the energy storage and charge- discharge performance of borate glass-ceramics by adjusting the glass structure. *Ceramics International*. 2022;48(4):5404–5412. Available from: https://doi.org/10.1016/j.ceramint.2021.11.084.
3) Alrowaili ZA, Ali AM, Baradi AMA, Al-Buriahi MS, Wahab EAA, Shaaban KS. A signifcant role of MoO3 on the optical, thermal, and radiation shielding characteristics of B2O3–P2O5–Li2O glasses. *Optical and Quantum Electronics* . 2022;54(88). Available from: https://doi.org/10.1007/s11082-021-03447-0.
4) Shaaban KS, Al-Baradi AM, Ali AM. Investigation of BaO reinforced TiO2–p2O5–li2O glasses for optical and neutron shielding applications. *RSC Advances*. 2022;12(5):3036–3043. Available from: https://dx.doi.org/10.1039/d2ra00171c.
5) Shaaban KS, Al-Baradi AM, Ali AM. Cr2O3 effect on the structure, optical, and radiation shielding properties of Na2B4O7–SiO2–CaO–Cr2O3 glasses. *Applied Physics A*. 2022;128(3). Available from: https://dx.doi.org/10.1007/s00339-022-05348-9.
6) Shaaban KS, Al-Baradi AM, Ali AM. Physical, optical, and advanced radiation absorption characteristics of cadmium lead phosphate glasses containing MoO3. *Journal of Materials Science: Materials in Electronics*. 2022;33(6):3297–3305. Available from: https://dx.doi.org/10.1007/s10854-021-07530-w.
7) Harizanova R, Slavov S, Vladislavova L, Costa LC, Avdeev G, Bocker C, et al. Barium titanate containing glass-ceramics - The effect of phase composition and microstructure on dielectric properties. *Ceramics International*. 2020;46(15):24585–24591. Available from: https://dx.doi.org/10.1016/j.ceramint.2020.06.247.
8) Shaaban KS, Al-Baradi AM, Ali AM. Physical, Mechanical, and Thermal Characteristics of B2O3 - SiO2- Li2O -Fe2O3 Glasses. *Silicon*. 2022. Available from: https://dx.doi.org/10.1007/s12633-022-01703-w.
9) Ramana EV, Prasad NV, Tobaldi DM, Zavašnik J, Singh MK, Hortigüela MJ, et al. Effect of samarium and vanadium co-doping on structure, ferroelectric and photocatalytic properties of bismuth titanate. *RSC Advances*. 2017;7(16):9680–9692. Available from: https://dx.doi.org/10.1039/c7ra00021a.
10) Liu Y, Fan L, Yi W, Yan C, Ma J, Ji Q, et al. Microstructure and ferroelectric properties of bi-excess Bi₄Ti₃O₁₂ thin films grown on Si and Pt/Ti/SiO₂/Si substrates. *Ferroelectrics*. 2020;554(1):144–149. Available from: https://dx.doi.org/10.1080/00150193.2019.1684756.
11) Thakur S, Vanita Thakur, Kaur A, Singh L. Study of the Crystallization and structural behavior of Bismuth Barium Titanate Glass-Ceramics. *Journal of Non-Crystalline Solids*. 2021;557:120563–120563. Available from: https://dx.doi.org/10.1016/j.jnoncrysol.2020.120563.
12) Nagaraju R, Devaiah B, Haritha L, Sekhar KC, Shareefuddin M, Sayed MA, et al. Influence of CaF2 on spectroscopic studies of lead fluoro bismuth borate glasses doped with Cr3+ ions. *Journal of Non-Crystalline Solids*. 2021;560:120705–120705. Available from: https://dx.doi.org/10.1016/j.jnoncrysol.2021.120705.
13) Bhemarajam J, Prasad P, Babu MM, Özcan M, Prasad M. Investigations on Structural and Optical Properties of Various Modifier Oxides (MO = ZnO, CdO, BaO, and PbO) Containing Bismuth Borate Lithium Glasses. *Journal of Composites Science*. 2021;5:308. Available from: https://doi.org/10.3390/jcs5120308.
14) Madheshiya A, Gautam C, Srivastava KK. Fabrication of lead-bismuth titanate borosilicate glass ceramics and dielectric characteristics doped with GNPs. *Materials Research Express*. 2020;7(1):015206–015206. Available from: https://dx.doi.org/10.1088/2053-1591/ab67ff.
15) Dubuis S, Messaddeq SH, Ledemi Y, Côté A, Messaddeq Y. Effect of Bi2O3 on the physical, structural and NIR emission properties of BGG glasses prepared using different melting atmospheres. *Optical Materials Express*. 2021;11(8):2560–2560. Available from: https://dx.doi.org/10.1364/ome.430811.
16) Reddy ASS, Kostrzewa M, Devi PPK, Purnachand N, Ingram A, Venkatramaiah N, et al. Dielectric dispersion impedance spectroscopy and polaron tunneling phenomenon in Au2O3 mixed PbO-B2O3-SeO2:Er2O3 glass ceramics. *Journal of Alloys and Compounds*. 2022;904:164069–164069. Available from: https://dx.doi.org/10.1016/j.jallcom.2022.164069.
17) Alajerami YS, Drabold DA, Mhareb MHA, Subedi KN, Cimatu KLA, Chen G. Physical, structural, and shielding properties of cadmium bismuth borate-based glasses. *Journal of Applied Physics*. 2020;127(17):175102–175102. Available from: https://dx.doi.org/10.1063/1.5143116.
18) Thomann H. A covalency model of ferroic phase transitions in perovskites. *Ferroelectrics*. 1987;73(1):183–199. Available from: https://dx.doi.org/10.1080/00150198708227917.
19) Sekhar KC, Shareefuddin M, El-Denglawey A, Saddeek YB. Structural and optical properties of BaTiO₃ modified cadmium alkali borate glasses. *Physica Scripta*. 2022. Available from: https://dx.doi.org/10.1088/1402-4896/ac53c7.
20) Sayed MA, Ali AM, El-Rehim AFA, Wahab EAA, Shaaban KS. Dispersion Parameters, Polarizability, and Basicity of Lithium Phosphate Glasses. *Journal of Electronic Materials*. 2021;50(6):3116–3128. Available from: https://dx.doi.org/10.1007/s11664-021-08921-9.
21) Naidu TM. Synthesis and characterization of Fe2O3-Bi2O3-TiO2nanoparticles and its magnetic properties. *Indian Journal of Science and Technology*. 2020;13(18):1848–1855. Available from: https://dx.doi.org/10.17485/ijst/v13i18.90.
22) Singh L, Vanita Thakur, Punia R, Kundu RS, Singh A. Structural and optical properties of barium titanate modified bismuth borate glasses. *Solid State Sciences*. 2014;37:64–71. Available from: https://dx.doi.org/10.1016/j.solidstatesciences.2014.08.010.

23) Gautam C, Yadav AK, Singh AK. A Review on Infrared Spectroscopy of Borate Glasses with Effects of Different Additives. *ISRN Ceramics*. 2012;2012:1–17. Available from: https://dx.doi.org/10.5402/2012/428497.
24) Ahmed MR, Sekhar KC, Hameed A, Chary MN, Shareefuddin M. Role of aluminum on the physical and spectroscopic properties of chromium-doped strontium alumino borate glasses. *International Journal of Modern Physics B*. 2018;32(08):1850095–1850095. Available from: https://dx.doi.org/10.1142/s0217979218500959.
25) Das S, Madheshiya A, Gautam SS, Tripathy D, Gautam C. Dielectric and Impedance Spectroscopic Characteristics of Lead Calcium Titanate Borosilicate Glass Ceramics. *Glass Physics and Chemistry*. 2020;46(6):514–525. Available from: https://dx.doi.org/10.1134/s108765962101003x.
26) Zhao Z, Liang X, Zhang T, Hu K, Li S, Zhang Y. Effects of cerium doping on dielectric properties and defect mechanism of barium strontium titanate glass-ceramics. *Journal of the European Ceramic Society*. 2020;40(3):712–719. Available from: https://dx.doi.org/10.1016/j.jeurceramsoc.2019.10.023.